Point-augmented biquadratic C^1 subdivision surfaces

Kęstutis Karčiauskas[a] and Jörg Peters[b]
[a] Vilnius University [b] University of Florida

Abstract

Shape artifacts, especially for convex input polyhedra, make Doo and Sabin's generalization of bi-quadratic (bi-2) subdivision surfaces unattractive for general design. Rather than tuning the eigenstructure of the subdivision matrix, we improve shape by adding a point and enriching the refinement rules. Adding a guiding point can also yield a polar bi-2 subdivision algorithm. Both the augmented and the polar bi-2 subdivision are complemented by a new primal bi-2 subdivision scheme. All surfaces are C^1 and can be combined.

1. Introduction

Primal Catmull-Clark subdivision (CC, [CC78]) and dual Doo-Sabin subdivision (DS, [DS78]) surfaces were introduced back-to-back in 1978 in order to extend smooth surfaces beyond tensor-product control nets. CC subdivision allows extraordinary control points where $n \neq 4$ quadrilaterals meet. DS subdivision allows extraordinary facets with $n \neq 4$ vertices.

CC subdivision has been widely popular with artists in the entertainment industry. Interpretation of the vertices of a regular CC mesh as control points of bi-cubic (bi-3) tensor-product B-splines yields a surface with smoothly-varying normals almost everywhere. By contrast, DS subdivision has not seen main-stream applications. This can be blamed on the underlying bi-2 tensor-product B-splines whose parameter lines join less gracefully: the normals vary only continuously between polynomial pieces and the images of parameter-lines are piecewise parabolas so that inflections along parameter lines can only occur at joints. However, more damaging are the under-documented shape defects near the facet-center limit points of DS subdivision Fig. 1b,d.

The goal of this paper is to revisit and rehabilitate Doo-Sabin subdivision near these extraordinary points. Sophisticated tuning strategies have been developed in the literature [PU98b, PU98a, ADS06] to improve the eigenspectrum near extraordinary points. By contrast, we aim to improve Doo-Sabin subdivision by adding a point and enriching the refinement rules. Our interest was triggered by recent high-quality multi-sided spline constructions based on guide surfaces (e.g. [KP13]). This approach uses the characteristic map and the extraordinary point of CC subdivision. Bi-2 subdivision would provide a simpler instance, on which to base a G^1 construction. Unfortunately, the strong artifacts of Doo-Sabin subdivision mean that the subdivision itself has to be improved before its components can be used.

Our second goal was to extend bi-2 subdivision to operate naturally on quad meshes; and to adapt it to a polar layout suitable for high valences. That is, the contributions of this submission are:

- Introducing a new point-augmented subdivision approach to remove artifacts present in Doo-Sabin subdivision (Fig. 2a);
- Adapting bi-2 subdivision to be primal, quad-based (Fig. 2b);
- Introducing bi-2 subdivision for polar configurations (Fig. 2c).

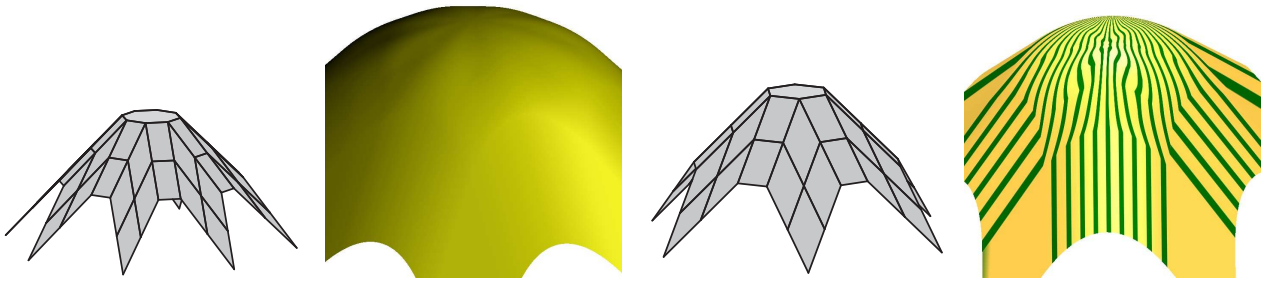

(a) Convex, $n = 8$ (b) Oscillation near and flatness at central point (c) Convex, $n = 6$ (d) Highlight lines

Figure 1: **Doo-Sabin subdivision artifacts:** (b) plain rendering shows artifacts for $n = 8$ and (d) highlight shading reveals them for $n = 6$.

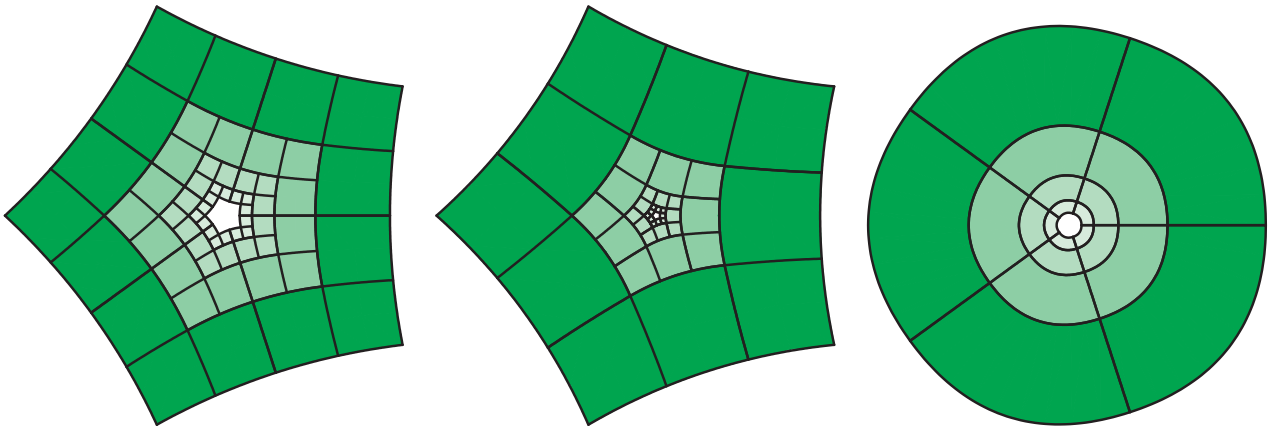

(a) DS: Doo-Sabin subdivision (b) TPS: Primal Bi-2 Subdivision (c) PolBS: Polar Bi-2 Subdivision

Figure 2: Nested **characteristic rings** of the three bi-2 subdivision algorithms developed in this paper.

Overview. Section 2 motivates, describes and analyzes the new Point-Augmented Bi-2 Subdivision devised to improve Doo-Sabin subdivision. Section 3 adds Polar Bi-2 Subdivision and Section 4 presents Primal Bi-2 Subdivision, a variant suitable for operating directly on quad meshes.

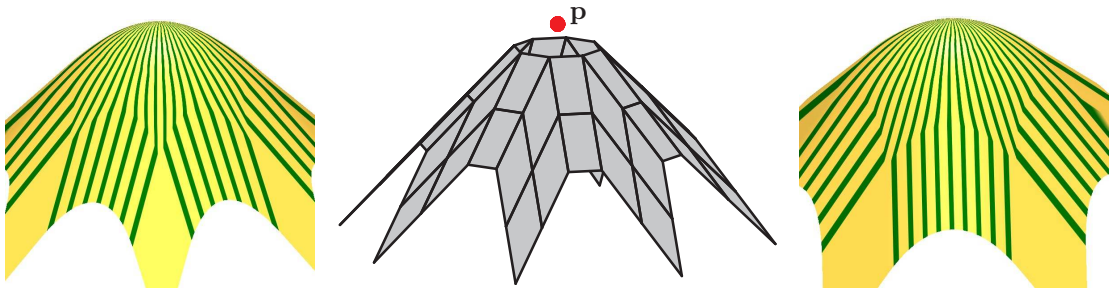

(a) PGS on input Fig. 1a (b) point added (c) PGS on input Fig. 1c

Figure 3: **Point-Augmented Bi-2 Subdivision**. The control-nets are minimal, defining just one regular bi-2 ring.

2. Point-Augmented Bi-2 Subdivision

The shape artifacts of Doo-Sabin subdivision (DS) include, for convex input, flatness at the extraordinary point and oscillation nearby (see Fig. 1). These and many other examples suggest that information is missing near the facet center. Our remedy is to add a central point $\mathbf{p}$ to the original control-net, see e.g. Fig. 3b. Such an additional point could be treated as a user-accessible shape parameter. However, $\mathbf{p}$ is extremely difficult to set by hand without damaging the surface quality.

Both for derivation and analysis, we view subdivision as a recipe for generating a sequence of nested surface rings (see Fig. 2). In Fig. 4, black disks denote the standard control-net of Doo-Sabin subdivision, the *DS-net*. Labels per sector, the point $\mathbf{p}$ and one (green) ring of regular bi-2 patches are displayed. Superscripts will indicate the subdivision level; but wherever it is unabiguous, we omit the superscript.

Structural symmetry and simplicity imply that $\mathbf{p}$ be a linear combination of the averages of the control points closest to the center:

$$\mathbf{p} := \mathbf{p}^0 := \mu_n \bar{\mathbf{a}}^0 + (1-\mu)\frac{\bar{\mathbf{b}}^0 + \bar{\mathbf{d}}^0}{2}, \quad \mu_n := \begin{cases} 3/5, & n = 3, \\ 2\frac{n-2}{n}, & n \geq 4. \end{cases} \tag{1}$$

$$\bar{\mathbf{a}}^k := \sum_{i=0}^{n-1} \mathbf{a}_i^k/n, \qquad \bar{\mathbf{b}}^k := \sum_{i=0}^{n-1} \mathbf{b}_i^k/n, \qquad \bar{\mathbf{d}}^k := \sum_{i=0}^{n-1} \mathbf{d}_i^k/n. \tag{2}$$

The key lies in setting μ_n. We determined μ_n to be simple while matching values that optimize reflection lines over a large set of challenging input nets. As intended, this choice extrapolates convex DS-nets when $n > 4$.

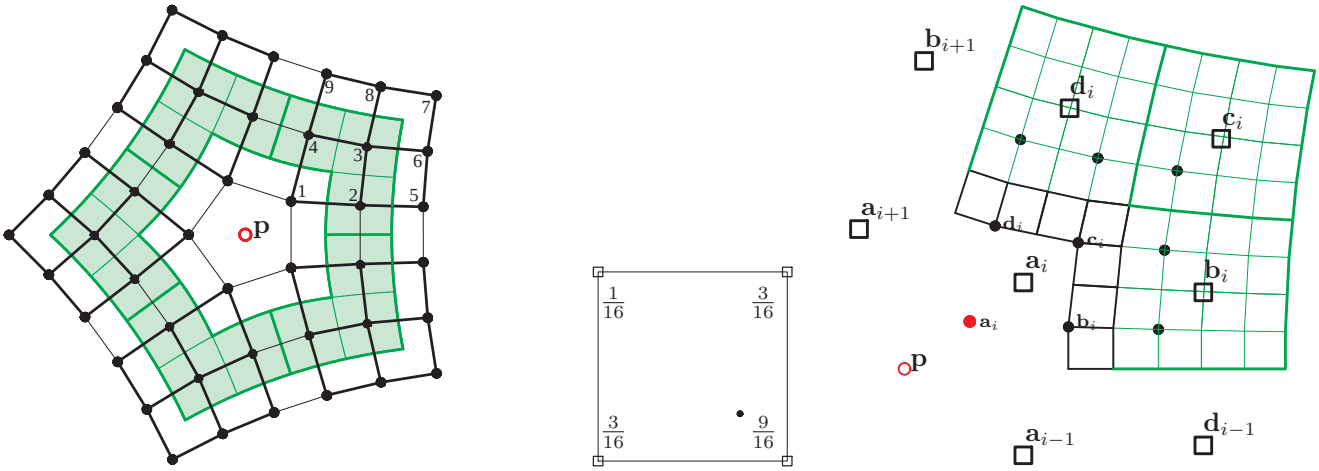

(a) DS-net + point $\mathbf{p}$ (b) regular bi-2 subdivision rule (c) refinement labels

Figure 4: **Labeling** Point-Augmented Bi-2 Subdivision. (a) One ring of bi-2 patches is shown in green. (b) The current control points □ with large labels and the refined control points • with small labels.

We derive the **refinement rules** of the new Point-Augmented Bi-2 Subdivision (PGS) by splitting the regular bi-2 patches into 2×2 subpatches in Bernstein-Bézier form (BB-form). Their inner BB-coefficients are the points of the refined control net, e.g. those marked as black disks with labels $5, \ldots, 9$ in Fig. 4a. New points $\mathbf{b}, \mathbf{c}, \mathbf{d}$, labelled $2, 3, 4$ in Fig. 4a are obtained as inner BB-coefficients of bi-2 patches that C^1-extend the existing bi-2 complex towards the center, i.e. the stencils are those of standard binary refinement. With α, w_1, w_2 still to be determined by (8), (9), (10), the added point, its n direct neighbors $\mathbf{a}$ (labelled 1 in Fig. 4a) and its indirect neighbors are set to

$$\mathbf{p}^{new} := (1-\alpha)\mathbf{p} + \alpha\overline{\mathbf{a}}, \tag{3}$$

$$\mathbf{a}_i^{new} := (1 - w_1 - 2w_2)\mathbf{p} + w_1\mathbf{a}_i + w_2(\mathbf{a}_{i-1} + \mathbf{a}_{i+1}). \tag{4}$$

$$\mathbf{b}_i^{new} := (9\mathbf{a}_i + 3\mathbf{a}_{i-1} + 3\mathbf{b}_i + \mathbf{d}_{i-1})/16, \quad \mathbf{d}_i^{new} := (9\mathbf{a}_i + 3\mathbf{a}_{i+1} + 3\mathbf{d}_i + \mathbf{b}_{i+1})/16.$$

Standard analysis of subdivision schemes following [PR08] applies the Discrete Fourier Transform to the $10n \times 10n$ circulant subdivision matrix A (where $\mathbf{p}/n$ is replicated n times). With the k-th Fourier block denoted by $\hat{A}_k$, the characteristic polynomials $D_k(\lambda)$ of $\hat{A}_k$ are, up to constant scaling, with $d(\lambda) := (\lambda - \frac{1}{4})(\lambda - \frac{1}{8})(\lambda - \frac{1}{16})\lambda^5$,

$$D_0(\lambda) = (\lambda - 1)d(\lambda)(\lambda - w_1 - 2w_2 + \alpha)\,; \tag{5}$$

$$\text{for } k = 1 \ldots n-1 \quad \mathsf{c}_k := \cos(2\pi k/n),$$

$$D_k(\lambda) = d(\lambda)\lambda(\lambda - w_1 - 2w_2\mathsf{c}_k). \tag{6}$$

The eigenvalue $\lambda_{sub} := w_1 + 2w_2\mathsf{c}_1$ of the blocks $\hat{A}_1$ and $\hat{A}_{n-1}$ is subdominant for suitable choice of w_1, w_2 and the corresponding characteristic ring (map) is injective (as will be clear by substituting λ_{sub} from (10) for λ in the expression [PR08, 6.21, p118]). The limit of the central point is computed from the left eigenvector of the eigenvalue 1 (see e.g. [HKD93]):

$$eop := (1-\tau)\mathbf{p} + \tau\overline{\mathbf{a}}_i, \quad \tau := \frac{\alpha}{1 + \alpha - w_1 - 2w_2}\,. \tag{7}$$

We now set the parameters α, w_1, w_2. As shown in the Appendix, the rules for mapping a DS-net to a new DS-net in their current general form are non-stationary. The two choices $\mu = 1$ or $\omega = 1$ for obtaining stationary rules yield poor shape already for simple examples. Therefore, to obtain stationary rules, we fix

$$\alpha := \frac{3}{4} + \mu_n(w_1 + 2w_2 - 1). \tag{8}$$

By our choice of w_1 and w_2 below, this makes formula (3) for $\mathbf{p}^{new}$ a convex combination, pulling towards, but not interpolating $\mathbf{p}^{init}$. The ratio $\frac{w_2}{w_1} = \frac{1}{4}$ is the simplest choice to match bi-quadratic subdivision, i.e. when $n = 4$. Since $\lambda_{sub} = w_1 + 2w_2\mathsf{c}$ by the earlier eigenanalysis, our choice

$$w_2 := \frac{w_1}{4}, \qquad w_1 := \frac{2\lambda_{sub}}{2 + \mathsf{c}}, \quad \mathsf{c} := \cos\frac{2\pi}{n}, \tag{9}$$

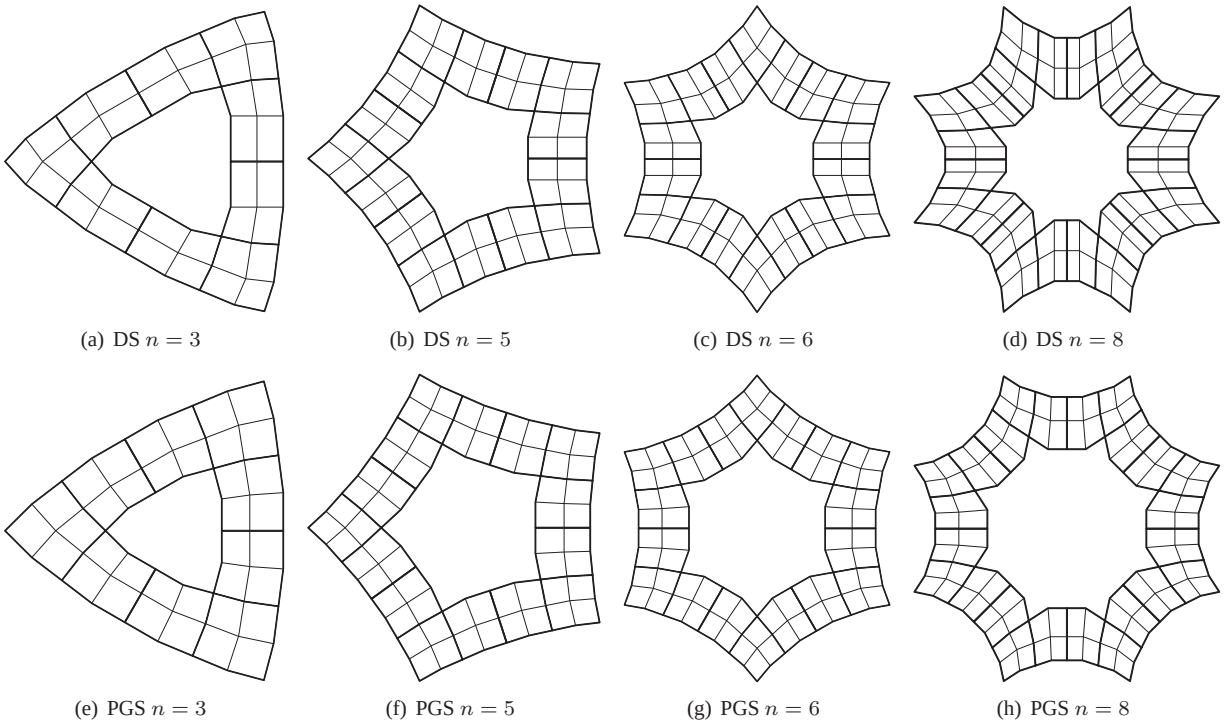

(a) DS $n = 3$ (b) DS $n = 5$ (c) DS $n = 6$ (d) DS $n = 8$

(e) PGS $n = 3$ (f) PGS $n = 5$ (g) PGS $n = 6$ (h) PGS $n = 8$

Figure 5: **Characteristic rings** of (*top*) Doo-Sabin subdivision, (*bottom*) Point-Augmented Bi-2 Subdivision.

is equivalent to prescribing λ_{sub}, i.e. the contraction speed of the characteristic rings. Mimicking the characteristic map of Catmull-Clark subdivision, we found a good choice to be

$$\lambda_{sub} := \sum_{i=0}^{3} b_i \binom{3}{i} (1-\mathsf{c})^{3-i}\mathsf{c}^i, \quad \mathsf{c} := \cos\frac{2\pi}{n}, \tag{10}$$

$$b_0 := \frac{1}{2},\ b_1 := 0.5519,\ b_2 := 0.5985,\ b_3 := 0.64367.$$

This yields the following subsubdominant eigenvalue ν_n for valence n: $\nu_3 = 1/4$; ν_5 and ν_6 are $w_1 + 2w_2 - \alpha$, a root of D_0 of (5); and for $n > 6$, $\nu_n = w_1 + 2w_2\mathsf{c}_2$, a root of D_2 of (6). Fig. 5 compares the characteristic rings of DS and PGS. While the subdominant eigenvalue of DS is 0.5, the subdominant eigenvalue of PGS exceeds 0.5 for $n > 4$, slowing down the central contraction.

2.1. Testing PGS

From a user's point of view, the input nets of DS and PGS are identical since the point $\mathbf{p}$ is added automatically. Hence, except for Fig. 3b, we display standard DS-nets. Compared to DS, PGS improves not only the shape for convex input (Fig. 3), but also saddle configurations (Fig. 6).

Prisms show shortcomings of both the DS and, to a lesser degree, of PGS. The oscillations in the highlight lines in Fig. 7e-g are caused by the three-sided faces introduced by the first DS refinement step (see Fig. 7b). As reported in [DS78], Catmull and Clark had suggested DS$^{\text{CC}}$ stencils, different from DS stencils (see Fig. 7d). DS$^{\text{CC}}$ has a worse eigenstructure at the extraordinary point than its DS improvement, but DS$^{\text{CC}}$ rules appear to be better at pre-processing coarse meshes: pre-processing the mesh with two steps of DS$^{\text{CC}}$ in lieu of DS (see Fig. 7c,d) before applying PGS improves the highlight lines as illustrated in Fig. 7e,f,g. Nevertheless, the results for prisms are unsatisfactory. This motivates the following polar construction.

3. Polar Bi-2 Subdivision

We can redesign prism nets and other cylindrical structures by introducing subnets with *polar layout* [KP07], shown in Fig. 8. Adding the poles as points $\mathbf{p}$ prevents the creation of irregular control-points of valence 3 on the prism top and bottom, see Fig. 8a. The placement of $\mathbf{p}$ can be as simple as the centroid of the multi-sided face. Unlike PGS, the point $\mathbf{p}$ of the new C^1 Polar Bi-2 Subdivision (PolBS) can be set by hand to modify shape without introducing obvious shape artifacts (see Fig. 8c,d).

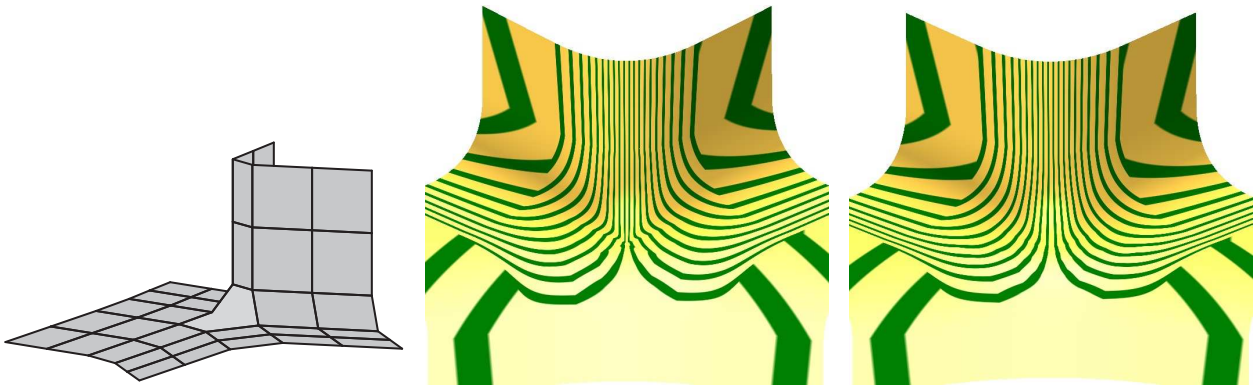

(a) input, $n = 6$ (b) DS (c) PGS

Figure 6: **Saddle configuration** with highlight shading.

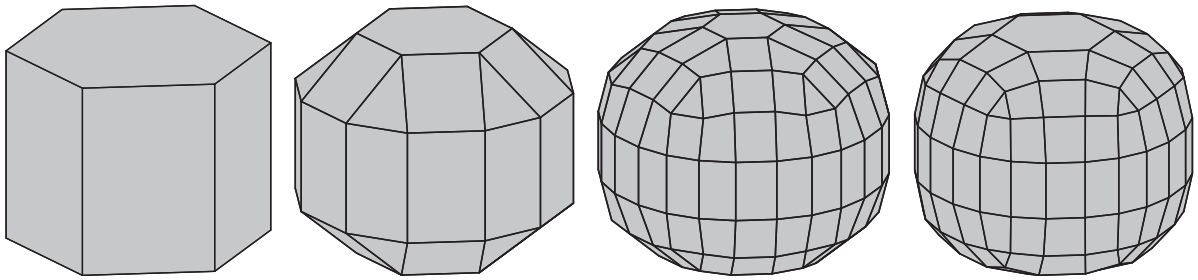

(a) $n = 6$ prism (b) DS $\times 1$ (c) DS $\times 2$ (d) DS^{CC} $\times 2$

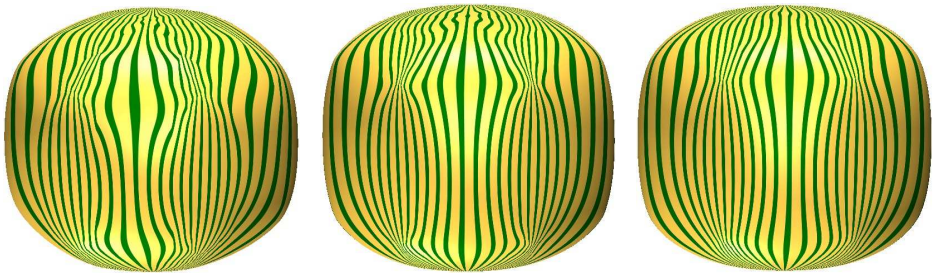

(e) DS of (a) (f) DS of (d) (g) PGS of (d)

Figure 7: **Prism** comparison. (d) Two steps of DS^{CC}.

PolBS is derived by adapting the approach of bi-3 polar subdivision [KP07]. The net of depth three surrounding $\mathbf{p}$ (see Fig. 9a). defines the green ring of bi-2 patches. Its control points in each sector are labelled $\mathbf{a}, \mathbf{b}, \mathbf{c}$. With the notation of Fig. 9b, we derive the refinement rules by first radially splitting the bi-2 patches of the ring; the resulting inner BB-coefficients, marked as blue disks, are the points of the refined polar control net with the label 3. C^1 extension towards the pole yields points of the refined net with the label 2. Since the bi-2 patches were only split radially, both type 2 and 3 points result from standard binary *one-dimensional* subdivision:

$$\mathbf{b}_i^{new} := \frac{3}{4}\mathbf{a}_i + \frac{1}{4}\mathbf{b}_i, \quad \mathbf{c}_i^{new} := \frac{1}{4}\mathbf{a}_i + \frac{3}{4}\mathbf{b}_i.$$

For $\gamma_{n-j} = \gamma_j,\ j = 1, \ldots, n-1$ determined in (15), the important new points labelled 1 (red disk in Fig. 9b) and the point $\mathbf{p}$ are set to

$$\mathbf{a}_i^{new} := (1 - \sum_{j=0}^{n-1} \gamma_j)\mathbf{p} + \sum_{j=0}^{n-1} \gamma_j \mathbf{a}_{i+j}, \tag{11}$$

$$\mathbf{p}^{new} := (1 - \alpha)\mathbf{p} + \alpha \bar{\mathbf{a}}_i. \tag{12}$$

Applying the Discrete Fourier Transform to the $4n \times 4n$ subdivision matrix A (where $\mathbf{p}/n$ is replicated n times), we obtain

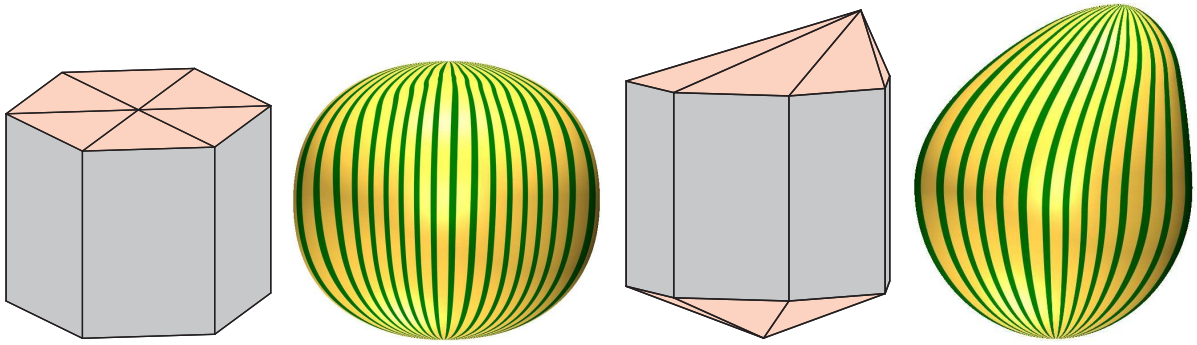

(a) $n = 6$ prism (b) PolBS (c) $n = 7$ prism (d) PolBS

Figure 8: **Polar Bi-2 Subdivision**: C^1 bi-2 polar subdivision surfaces. (c) the default centroids of the 7-sided prism have been moved.

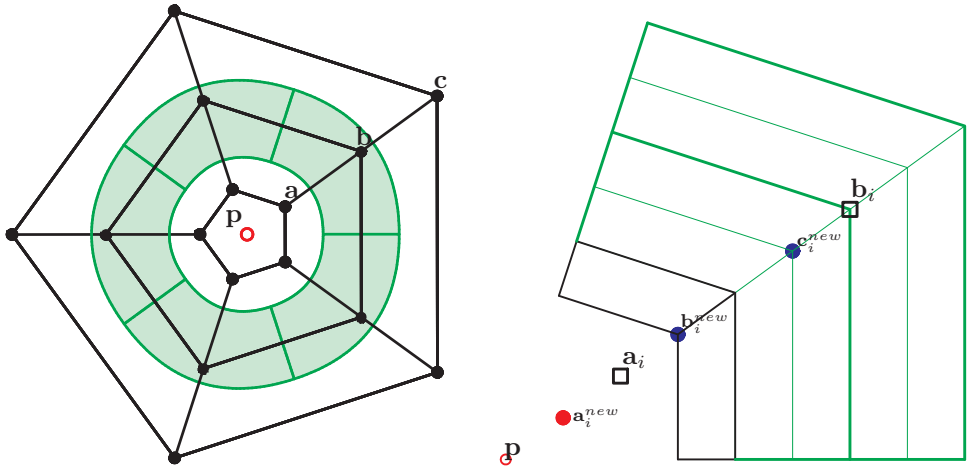

(a) Polar layout (b) Polar refinement

Figure 9: **Polar Bi-2 Subdivision** layout and refinement.

characteristic polynomials $D_k(\lambda)$ of $\hat{A}_k$ that are, up to constant scaling

$$D_0(\lambda) = (\lambda - 1)(\lambda - \frac{1}{4})\lambda(\lambda - \beta + \alpha); \qquad \beta := \sum_{j=0}^{n-1} \gamma_j, \tag{13}$$

for $k = 1 \ldots n-1$,

$$D_k(\lambda) = (\lambda - \frac{1}{4})\lambda^2(\lambda - \hat{\gamma}_k), \qquad \hat{\gamma}_k := \sum_{j=0}^{n-1} \gamma_j \cos\Big(\frac{2\pi}{n} kj\Big). \tag{14}$$

Inverting (14) for γ_j as in [Loo02] and noting that $\beta = \hat{\gamma}_0$, we set in the spirit of [KP07]

$$\alpha := \frac{1}{4} \text{ and } \hat{\gamma}_j := \begin{cases} 1/2, & j \in \{0, 1, n-1\} \\ 0, & \text{else,} \end{cases} \qquad \text{and this yields}$$

$$\gamma_k = \frac{1}{n} \sum_{j=0}^{n-1} \hat{\gamma}_j \cos\Big(\frac{2\pi}{n} kj\Big) = \frac{1}{n}\Big(\frac{1}{2} + \mathsf{c}_k\Big), \qquad \beta = \frac{1}{2}. \tag{15}$$

The eigenspectrum satisfies the C^1 requirements, since $\hat{\gamma}_1 = \hat{\gamma}_{n-1} = \frac{1}{2}$ and $\hat{\gamma}_k = 0$ for $k = 2, \ldots, n-2$. In particular, the subdominant eigenvalue is $1/2$ and the subsubdominant eigenvalue is $1/4$. The characteristic map is, in the circular direction, a periodic C^1 spline of degree 2, and is linear in the radial direction; it is injective. The eigenanalysis shows the limit extraordinary point to be

$$eop := \frac{2}{3}\mathbf{p} + \frac{1}{3}\bar{\mathbf{a}}. \tag{16}$$

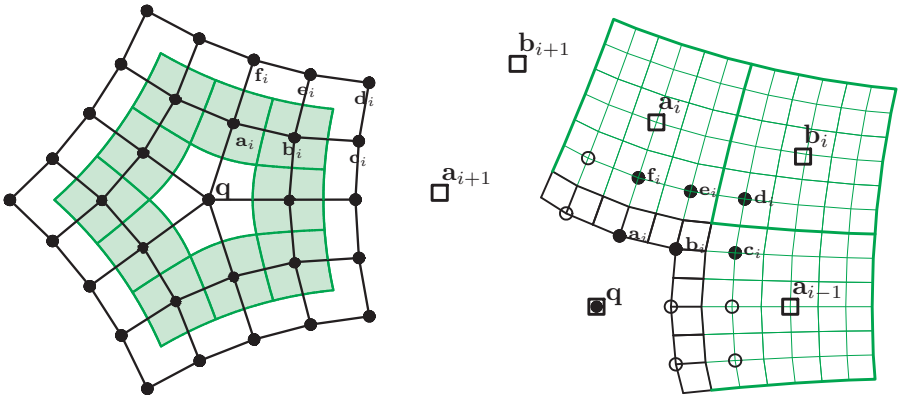

(a) q-net-labels (b) ternary refinement

Figure 10: **Primal Bi-2 Subdivision**. (b) Smaller fonts label refined control points.

4. Primal Bi-2 Subdivision

A single step of CC subdivision converts any mesh into a quad net suitable for Primal Bi-2 Subdivision (TPS). We consider a net of depth three surrounding the central point $\mathbf{q}$ and call it q-net (see Fig. 10a). Such a q-net defines one ring of bi-2 patches. Its control points in each sector are labelled $\mathbf{a}_i, \ldots, \mathbf{f}_i$.

To derive the refinement rules of TPS, the bi-2 patches of the green ring are split into 3×3 subpatches. Their new inner BB-coefficients, marked as black circles, are the points labelled $\mathbf{c}, \mathbf{d}, \mathbf{e}, \mathbf{f}$ of the refined control net. C^1-extension towards the center yields points of the refined net with the labels $\mathbf{a}$ and $\mathbf{b}$. The formulas are those of ternary bi-2 subdivision (hence the T in TPS):

$$\begin{aligned}
\mathbf{a}_i^{new} &:= (14\mathbf{q} + 7\mathbf{a}_i + 2(\mathbf{a}_{i-1} + \mathbf{a}_{i+1}) + \mathbf{b}_i + \mathbf{b}_{i+1})/27;\\
\mathbf{b}_i^{new} &:= (4\mathbf{q} + 2\mathbf{a}_i + 2\mathbf{a}_{i-1} + \mathbf{b}_i)/9\ ;\\
\mathbf{c}_i^{new} &:= (4\mathbf{a}_{i-1} + 2\mathbf{q} + 2\mathbf{b}_i + \mathbf{a}_i)/9\ ;\\
\mathbf{d}_i^{new} &:= (4\mathbf{b}_i + 2\mathbf{a}_i + 2\mathbf{a}_{i-1} + \mathbf{q})/9;\\
\mathbf{e}_i^{new} &:= (4\mathbf{a}_i + 2\mathbf{b}_i + 2\mathbf{q} + \mathbf{a}_{i-1})/9;\\
\mathbf{f}_i^{new} &:= (14\mathbf{a}_i + 7\mathbf{q} + 2(\mathbf{b}_i + \mathbf{b}_{i+1}) + \mathbf{a}_{i-1} + \mathbf{a}_{i+1})/27.
\end{aligned} \tag{17}$$

We set

$$\mathbf{q}^{new} := (1 - \alpha_1 - \alpha_2)\mathbf{q} + \alpha_1\overline{\mathbf{a}} + \alpha_2\overline{\mathbf{b}}. \tag{18}$$

For the presented scheme, standard analysis of subdivision schemes following [PR08] applies the Discrete Fourier Transform to the $7n \times 7n$ circulant subdivision matrix A (where $\mathbf{q}/n$ is replicated n times). The characteristic polynomials $D_k(\lambda)$ of $\hat{A}_k$ are, up to constant scaling,

$$D_0(\lambda) = (\lambda - 1)\lambda^4\Big(\lambda^2 + (\alpha_1 + \alpha_2 - \frac{14}{27})\lambda + \frac{1}{81}(1 - 3\alpha_1 + 3\alpha_2)\Big); \tag{19}$$

$$\text{for } k = 1 \ldots n-1, \qquad \mathsf{c}_k := \cos\frac{2\pi k}{n},$$

$$D_k(\lambda) = \lambda^5\Big(\lambda^2 - \frac{2}{27}(5 + 2\mathsf{c}_k)\lambda + \frac{1}{81}\Big). \tag{20}$$

From the left eigenvector of the dominant eigenvalue 1, we obtain the limit point

$$\begin{aligned}
eop &:= (1 - \tau_1 - \tau_2)\mathbf{q} + \tau_1\overline{\mathbf{a}}_i + \tau_2\overline{\mathbf{b}}_i,\\
&\text{where } \tau_1 := \frac{18(2\alpha_1 + \alpha_2)}{39\alpha_1 + 42\alpha_2 + 20}, \quad \tau_2 := \frac{3(\alpha_1 + 8\alpha_2)}{39\alpha_1 + 42\alpha_2 + 20}.
\end{aligned} \tag{21}$$

The parameters α_1 and α_2 for $n > 4$ are chosen by experiment to generalize the regular case when $n = 4$:

$$\alpha_1 := \frac{7n}{(2n+1)^2}\ , \quad \alpha_2 := \frac{\alpha_1}{7}.$$

For $n = 3$, also obtained by experiment, we set $\alpha_1 := \frac{339}{896}$, $\alpha_2 := \alpha_1/7$. Then the scheme is C^1 with subdominant eigenvalue λ from $\hat{A}_1$, $\hat{A}_{n-1}$

$$\lambda = \frac{1}{27}\left(5 + 2\mathsf{c} + 2\sqrt{\mathsf{c}^2 + 5\mathsf{c} + 4}\right), \quad \mathsf{c} := \cos\frac{2\pi}{n},$$

and a subsubdominant eigenvalue of $\nu_3 = .082$, the larger root of D_0 in (19) and $\nu_n = (5 + 2\mathsf{c}_2 + 2\sqrt{\mathsf{c}_2^2 + 5\mathsf{c}_2 + 4})/27$ for higher valences and $\mathsf{c}_2 := \cos\frac{\pi}{n}$. We checked numerically up to valence 100 that the characteristic map is injective. Fig. 11 shows the BB-coefficients of the characteristic rings for often-used valencies. Fig. 12 highlights the shape for convex as well as for saddle input data.

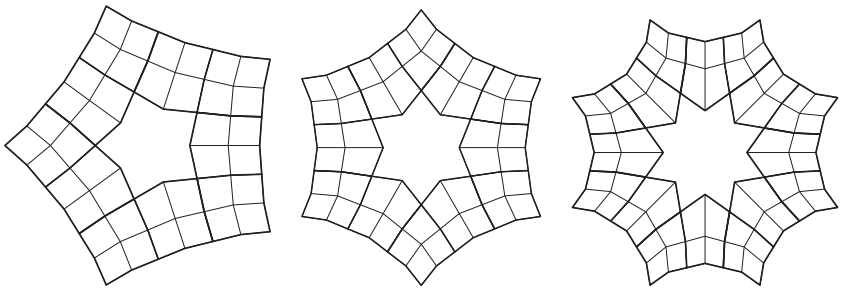

(a) TPS $n = 5$ (b) TPS $n = 6$ (c) TPS $n = 8$

Figure 11: Bézier coefficients of **characteristic rings** of Primal Bi-2 Subdivision.

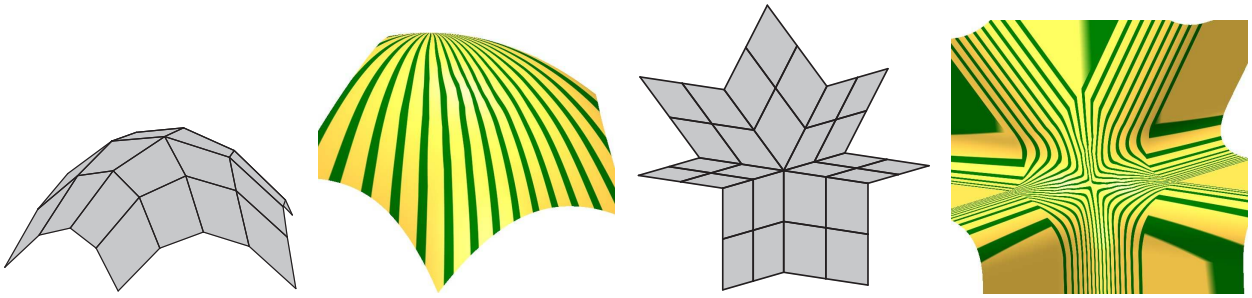

(a) q-net $n = 5$ (b) TPS convex (c) q-net $n = 7$ (d) TPS saddle

Figure 12: **Primal Bi-2 Subdivision** surfaces, (b) and (d) in highlight shading.

4.1. An adjustable TPS

Ternary subdivision contracts fast (see Fig. 2b). Indeed, the test cases indicate that the fast contraction can result in slight oscillations and faster-than-wanted direction changes of highlight lines. We can improve the surfaces by adjusting the refinement ratio as in [KP09]. Specifically, we split edges non-uniformly in the ratio $e : 1 - 2e : e$ so that $e := \frac{1}{3}$ yields the uniform case developed as TPS (cf. Fig. 13). We chose the free parameters α_1, α_2 so that the extraordinary point of adjustable TPS coincides with that of TPS. This avoids the flatness for convex control nets, often observed, e.g. when CC subdivision is tuned to contract more slowly.

The standard analysis of adjustable TPS yields the subdominant eigenvalue

$$\lambda := (1 - 2e)\left(e^2(1 + 2\mathsf{c}) + (1 - e)^2 + 2e\sqrt{(\mathsf{c} + 1)(e^2\mathsf{c} + (1 - e)^2)}\right). \tag{22}$$

Slowing the contraction, by setting $e := 0.2$ yields the characteristic rings shown in Fig. 13. Fig. 14 illustrates adjustment for $n = 9$.

5. Discussion

We used individualized heuristics for setting parameters such as α and w_i, rather than tuning the eigenstructure. Tuning is tricky due to too many free parameters – and while tuning formally satisfies smoothness constraints at the limit point it often decreases the surface quality in its neighborhood.

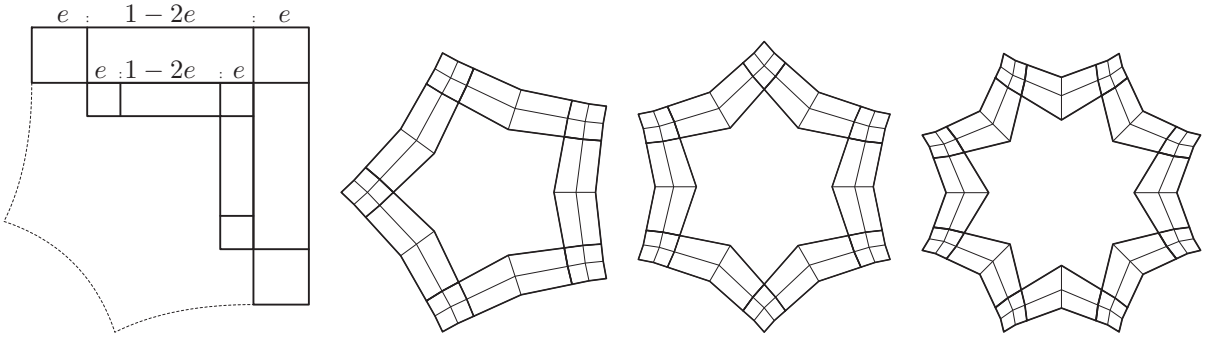

(a) ratio (b) $n = 5, e = 0.2$ (c) $n = 6, e = 0.2$ (d) $n = 8, e = 0.2$

Figure 13: Splitting ratio and BB-coefficients of characteristic rings of **adjustable TPS**.

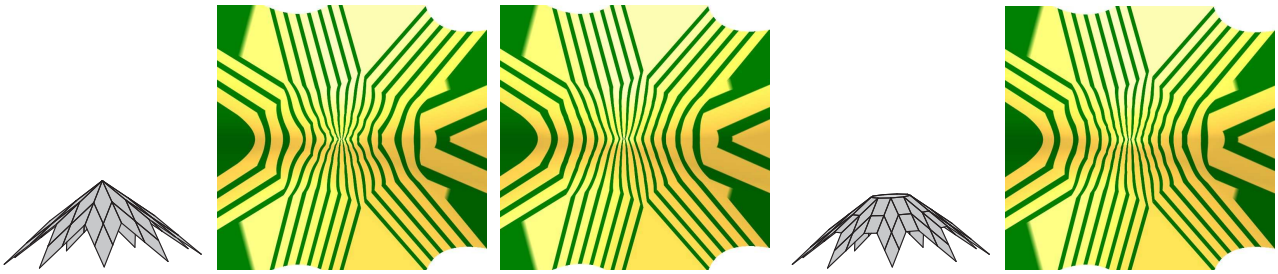

(a) q-net $n = 9$ (b) TPS on input (a) (c) adjustable TPS $e = 0.15$ on input (a) (d) q-net + DS (e) PGS on input (d)

Figure 14: Highlight line comparison on **convex input nets**. The q-net of (d) is obtained by applying one step of regular bi-2 subdivision to (a).

Setting α by (8) simplifies the analysis. It is possible that a non-stationary rule achieves equivalent or better surface quality.

We did test, without success, rules involving more p-net points for equation (2). We settled for adding a point since this provides stable convex combination rules as opposed to repeatedly extrapolating with positive and negative coefficients. Moreover, the augmented rules require fewer operations than more complex alternatives.

By treating the subdivision surfaces as a sequence of nested rings, it is possible to combine binary and ternary subdivision. The input mesh Fig. 15a is specially constructed to show such a combination, featuring regular bi-2 parts, TPS at the corner saddles and the central PGS surface. Since PGS is binary and TPS ternary, it is difficult to imagine how pure mesh refinement would cope with the situation.

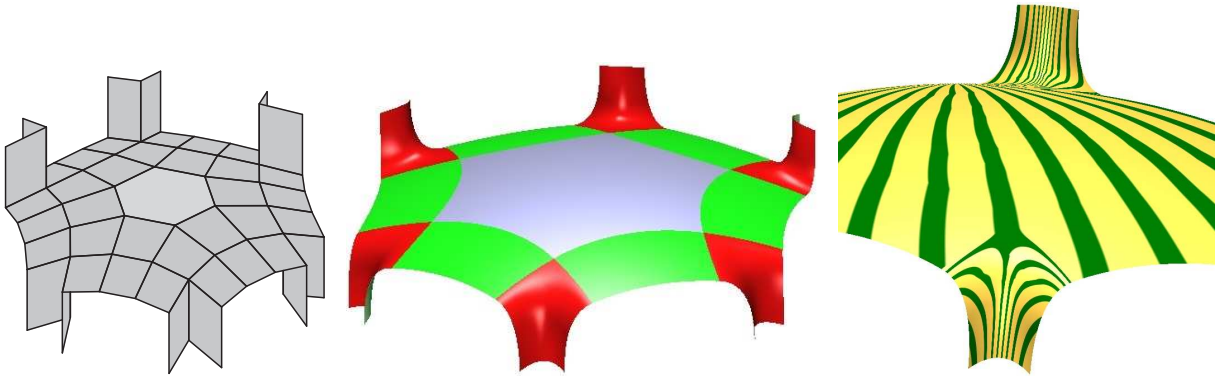

(a) input (b) surface regions (c) highlight shading

Figure 15: **Combining bi-2 subdivision** schemes: (a) Mesh with multi-sided face and multi-valent vertices. (b) regular bi-2 regions are green, PGS-region are grey, TPS-regions are red.

Overall, the addition of a judiciously chosen point $\mathbf{p}$ has markedly improved the shape of bi-2 subdivision surfaces for convex control nets compared to classical Doo-Sabin subdivision. Since no mathematical theory of good shape exists, we derived by experiment the extrapolation constant μ_n (as well as the convex combination weights $\alpha, \alpha_1, \alpha_2, \gamma_j, w_1$ and w_2 of

the various schemes). The addition of Primal Bi-2 Subdivision and Polar Bi-2 Subdivision, increases the applicability of bi-2 subdivision, making it a useful alternative where low polynomial degree matters.

Acknowledgements.. This work was supported in part by NSF grant CCF-1117695.

[ADS06] Ursula H. Augsdörfer, Neil A. Dodgson, and Malcolm A. Sabin. Tuning subdivision by minimising gaussian curvature variation near extraordinary vertices. *Comput. Graph. Forum*, 25(3):263–272, 2006.

[CC78] E. Catmull and J. Clark. Recursively generated B-spline surfaces on arbitrary topological meshes. *Computer-Aided Design*, 10:350–355, 1978.

[DS78] D. Doo and M. Sabin. Behaviour of recursive division surfaces near extraordinary points. *Computer-Aided Design*, 10:356–360, September 1978.

[HKD93] Mark Halstead, Michael Kass, and Tony DeRose. Efficient, fair interpolation using Catmull-Clark surfaces. In James T. Kajiya, editor, *Computer Graphics (SIGGRAPH '93)*, volume 27, pages 35–44, August 1993.

[KP07] Kęstutis Karčiauskas and Jörg Peters. Bicubic polar subdivision. *ACM Trans. Graph.*, 26(4):14, 2007.

[KP09] K. Karčiauskas and J. Peters. Adjustable speed surface subdivision. *Computer Aided Geometric Design.*, 26:962–969, 2009.

[KP13] K. Karčiauskas and J. Peters. Biquintic G^2 surfaces. *14th Itl Conference on Mathematics of Surfaces*, pages 213–236, Sept 2013.

[Loo02] C. Loop. Smooth ternary subdivision of triangle meshes. In *Proceedings of Curve and Surface Fitting*, pages 295–302, Saint-Malo, France, 2002.

[PR08] J. Peters and U. Reif. *Subdivision Surfaces*. Springer, 2008.

[PU98a] Hartmut Prautzsch and Georg Umlauf. A G2-subdivision algorithm. In *Proc. Geom. Model., Dagstuhl, Germany, 1996*, pages 217–224. Springer, 1998.

[PU98b] Hartmut Prautzsch and Georg Umlauf. Improved triangular subdivision schemes. In *Computer Graphics International*, pages 626–632. IEEE Computer Society, 1998.

Appendix: Stationarity of Point-Augmented Bi-2 Subdivision

Denoting $\mathbf{p}^0 := \mathbf{p}^{init}$ and $\omega := w_1 + 2w_2$, the kth Point-Augmented Bi-2 Subdivision subdivides the averages as

$$\mathbf{p}^{k+1} := (1-\alpha)\mathbf{p}^k + \alpha\overline{\mathbf{a}}^k, \quad \overline{\mathbf{a}}^{k+1} := (1-\omega)\mathbf{p}^k + \omega\overline{\mathbf{a}}^k,$$
$$\overline{\mathbf{b}}^{k+1} := (9\overline{\mathbf{a}}^k + 3\overline{\mathbf{a}}^k + 3\overline{\mathbf{b}}^k + \overline{\mathbf{d}}^k)/16, \quad \overline{\mathbf{d}}^{k+1} := (9\overline{\mathbf{a}}^k + 3\overline{\mathbf{a}}^k + 3\overline{\mathbf{d}}^k + \overline{\mathbf{b}}^k)/16.$$

For $k = 0$ and abbreviating $\kappa := (1-\omega)\mu + \omega$,

$$\overline{\mathbf{a}}^1 := (1-\omega)\mathbf{p}^0 + \omega\overline{\mathbf{a}}^0 = \kappa\overline{\mathbf{a}}^k + (1-\kappa)\frac{\overline{\mathbf{b}}^k + \overline{\mathbf{d}}^k}{2}. \tag{23}$$

For $k = 1$, we must therefore also have

$$(1-\omega)\mathbf{p}^k + \omega\overline{\mathbf{a}}^k = \overline{\mathbf{a}}^{k+1} = \kappa\overline{\mathbf{a}}^k + (1-\kappa)\frac{\overline{\mathbf{b}}^k + \overline{\mathbf{d}}^k}{2}. \tag{24}$$

By substituting (preferably using a symbolic manipulation program) $\mathbf{p}^k$, $\overline{\mathbf{a}}^k$, $\overline{\mathbf{b}}^k$ and $\overline{\mathbf{d}}^k$ in their subdivision form, (24) is equivalent to

$$(\mu-1)(2\overline{\mathbf{a}}^0 - \overline{\mathbf{b}}^0 - \overline{\mathbf{d}}^0)(\omega-1)(\mu\omega - \mu + 3/4 - \alpha) = 0.$$

(Further extensive symbolic computation, up to $n = 40$ showed conversely that (8) implies that the rules are stationary.)